nature medicine

BRIEF COMMUNICATION

https://doi.org/10.1038/s41591-018-0265-6

Corrected: Publisher Correction

Ultraviolet radiation–induced DNA damage is prognostic for outcome in melanoma

Lucas D. Trucco[1,5], Piyushkumar A. Mundra[1,5], Kate Hogan[1,5], Pablo Garcia-Martinez[1,5], Amaya Viros[1], Amit K. Mandal[1], Nicolas Macagno[2], Caroline Gaudy-Marqueste[3], Donald Allan[4], Franziska Baenke[1], Martin Cook[1], Clare McManus[1], Berta Sanchez-Laorden[1], Nathalie Dhomen[1] and Richard Marais[1*]

The melanoma genome is dominated by ultraviolet radiation (UVR)-induced mutations. Their relevance in disease progression is unknown. Here we classify melanomas by mutation signatures and identify ten recurrently mutated UVR signature genes that predict patient survival. We validate these findings in primary human melanomas; in mice we show that this signature is imprinted by short-wavelength UVR and that four exposures to UVR are sufficient to accelerate melanomagenesis.

Epidemiological and animal model studies have established an association between UVR exposure and melanoma[1,2], and cancer genome sequencing has revealed a predominance of C-to-T nucleotide transitions at dipyrimidines in common cutaneous melanoma[3–5]. This profile is also observed in UVR-exposed cells[6]. When considered in the trinucleotide context, a unique mutation pattern emerges that is known as signature 7, which prevails in UVR-associated skin cancers[7]. To investigate the relationship between signature 7 and melanoma progression, we analyzed cutaneous melanoma genomes from The Cancer Genome Atlas (TCGA)[3] by performing mutational spectrum analysis[7,8] on melanomas that originated on nonglabrous skin, but excluding acral and metastatic melanomas of unknown primary origin. We segregated the tumors depending on the predominance of signature 7, generating a cohort of 47 tumors in which signature 7 was absent or a negligible component (non–signature 7), and a second cohort of 372 tumors in which signature 7 predominated (signature 7) (Fig. 1a). We ranked the tumors in these cohorts by mutation load; on average the signature 7 cohort presented a higher number of single-nucleotide variants (SNVs; 961.8 versus 57.1, $P<0.0001$; Fig. 1b and Extended Data Fig. 1a) and a higher proportion of C-to-T transitions at dipyrimidines (mean: 84.7 versus 29.0%, $P<0.0001$; Fig. 1c and Extended Data Fig. 1b). We observed that the genes *LRP1B, ADGRV1, XIRP2, PKHD1L1, USH2A, DNAH9, PCDH15, DNAH10, TP53* and *PCDHAC1* were recurrently mutated in the signature 7 melanomas (Fig. 1d); hence, mutations in these genes correlated with an increased percentage of C-to-T transitions at dipyrimidines (Extended Data Fig. 1c). The majority of mutations carried by these ten genes were C-to-T substitutions at dipyrimidines (Extended Data Fig. 1d). Principal component analysis (PCA) confirmed signature 7 as the key component distinguishing the cohorts (Fig. 1e).

Intriguingly, compared to non–signature 7 patients, signature 7 patients presented longer disease-free ($P=0.0056$; Extended Data Fig. 1e) and better overall ($P<0.0001$;Fig. 1f) survival independent of disease stage at diagnosis (Extended Data Fig. 1f,g and Supplementary Table 1). Moreover, patients with tumors presenting a mutation in any of the ten signature-7-associated genes presented better overall survival than patients whose tumors lacked mutations in these genes ($P=0.0001$; Fig. 1g), and signature 7 was a better prognostic marker than mutation burden (Extended Data Fig. 1h,i). Using targeted sequencing, we validated mutations in the ten genes as prognostic of outcome in an independent cohort of primary cutaneous melanomas ($P=0.0013$; Fig. 1h and Supplementary Table 2). Signature 7 also predicted a trend toward favorable outcome in patients with melanoma undergoing immunotherapy[9,10] (Extended Data Fig. 1j). In silico predictions of major histocompatibility complex class I–binding mutated peptides showed that signature 7 melanomas presented more putative neoantigens[11] (Extended Data Fig. 2a–c). Moreover, gene expression–based immune-deconvolution analysis revealed that signature 7 melanomas presented an immune cell composition associated with better outcome[12], with higher estimated proportions of activated memory CD4 T cells and M1-polarized macrophages, but lower frequencies of monocytes (Extended Data Fig. 2d–g).

Solar UVR reaching the earth's surface is divided into UVA (320–400 nm) and UVB (280–320 nm)[13]. It is difficult to determine their individual contribution to melanomagenesis and signature 7 imprinting because of the variability of sunlight exposure in the genetically complex human population. Therefore, we used our $BRAF^{V600E}$-driven mouse melanoma model to examine this[14]. We previously reported that broad wavelength UVR (280–380 nm; $UV^{280–380}$) accelerated melanomagenesis in this model[15], so in this study we refined UVR exposure using different phototherapeutic lamps to compare broad, short (310–315 nm; $UVB^{310–315}$) and long (350–400 nm; $UVA^{350–400}$) wavelength UVR (Extended Data Fig. 3a). We induced $BRAF^{V600E}$ expression in the melanocytes of the mice and exposed half of their backs to UVR to provide contralateral exposed and protected skin for each animal (Extended Data Fig. 3b). Twenty-four hours after UVR exposure, we observed increased thymine dimers and p53 in the epidermal keratinocytes of mice exposed to $UV^{280–380}$ and $UVB^{310–315}$, but these DNA damage markers were absent in mice exposed to $UVA^{350–400}$ (Fig. 2a and Extended Data Fig. 3c).

To examine the consequences of long-term UVR exposure, mice induced to express $BRAF^{V600E}$ in their melanocytes were exposed to

[1]Molecular Oncology Group, Cancer Research UK Manchester Institute, University of Manchester, Manchester, UK. [2]Department of Pathology, Aix-Marseille University, APHM, Hôpital de la Timone, Marseille, France. [3]Dermatology and Skin Cancer Department, Aix-Marseille University, APHM, Hôpital de la Timone, Marseille, France. [4]Medical Physics Department and The University of Manchester, Manchester Academic Health Science Centre, Salford Royal NHS Foundation Trust, Salford, UK. [5]These authors contributed equally: Lucas D. Trucco, Piyushkumar A. Mundra, Kate Hogan, Pablo Garcia-Martinez. *e-mail: richard.marais@cruk.manchester.ac.uk

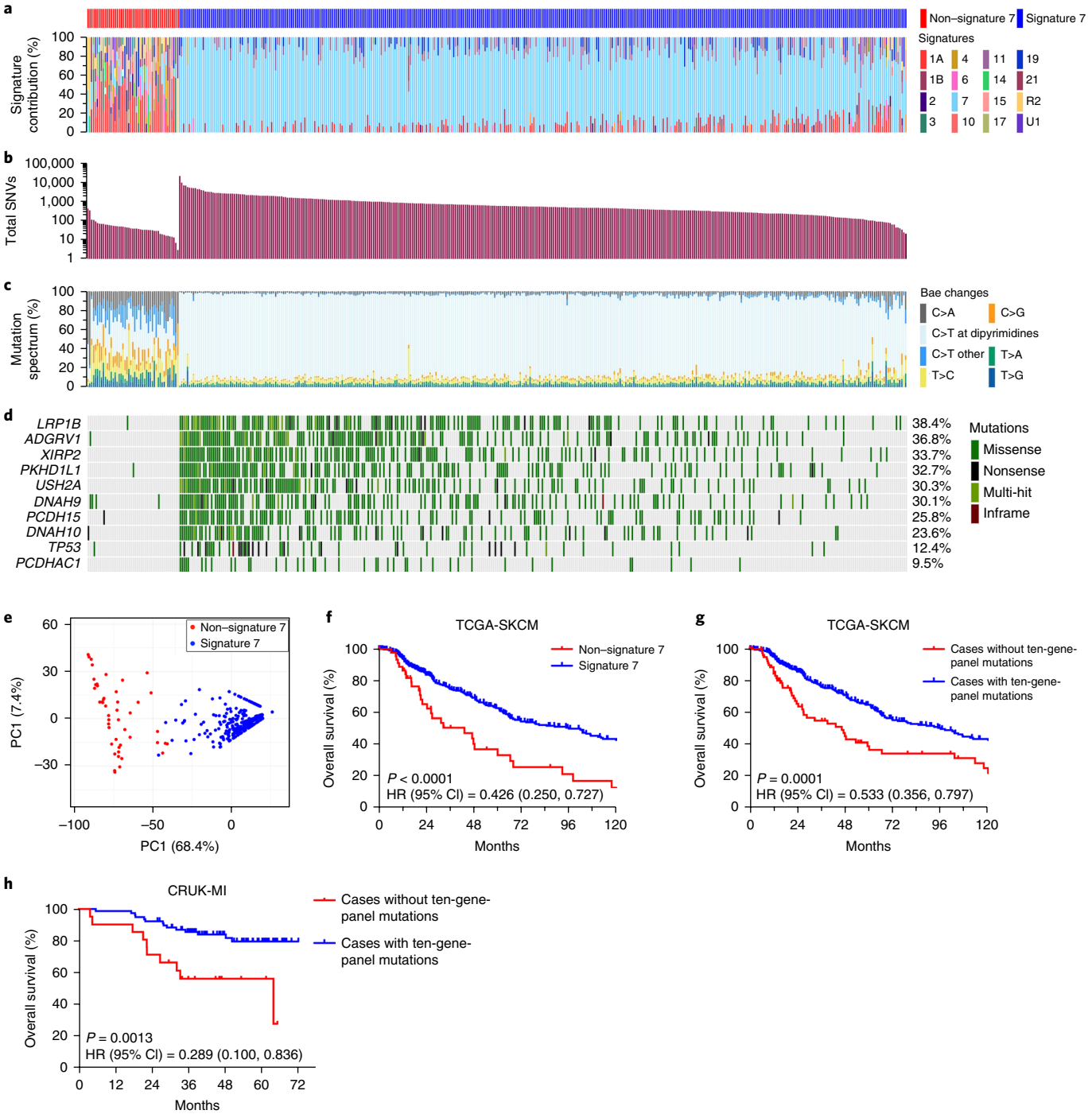

Fig. 1 | Signature 7 is prognostic for survival in cutaneous melanoma. a–**c**, Segregation of TCGA cutaneous melanomas according to predominance of signature 7. Plots represent the percentage of mutations attributed to each signature (**a**), total SNVs (**b**) and the spectrum of somatic base changes (**c**). **d**, Ten genes recurrently altered by nonsynonymous mutations in signature 7 tumors. **e**, PCA of mutational signature weights in TCGA melanomas ($n = 419$). The values in parentheses denote the percentage of variance explained. **f**, Overall survival of TCGA patients with cutaneous melanoma segregated by predominance of signature 7; $n = 419$, two-tailed log-rank test. HR, hazard ratio. **g**,**h**, Overall survival of melanoma patients from TCGA ($n = 419$) (**g**) and CRUK-MI ($n = 100$) (**h**) cohorts, classified according to the presence of mutations in one or more of the ten genes from **d**; two-tailed log-rank test. SKCM, skin cutaneous melanoma.

UVR once a week for up to 26 weeks (chronic UVR, Extended Data Fig. 4a). $UVB^{310–315}$ increased the size and number of intradermal naevi in $BRAF^{V600E}$-expressing mice, whereas $UVA^{350–400}$ increased the size but not the number of naevi (Extended Data Fig. 4b and Supplementary Table 3), a pattern replicated by tumor latency and burden. Specifically, non-UVR-exposed $BRAF^{V600E}$-expressing mice developed on average 0.9 tumors at a median latency of 30.5 weeks, whereas $BRAF^{V600E}$-expressing mice exposed to $UV^{280–380}$ or $UVB^{310–315}$ developed on average 2.8 melanomas ($P = 0.0003$) at a median latency of 20 weeks ($P \leq 0.0001$), and mice exposed to $UVA^{350–400}$ developed on average 1.3 melanomas ($P = 0.0621$) at a median latency of 43 weeks ($P = 0.293$; Fig. 2b,c). Melanoma did not develop in

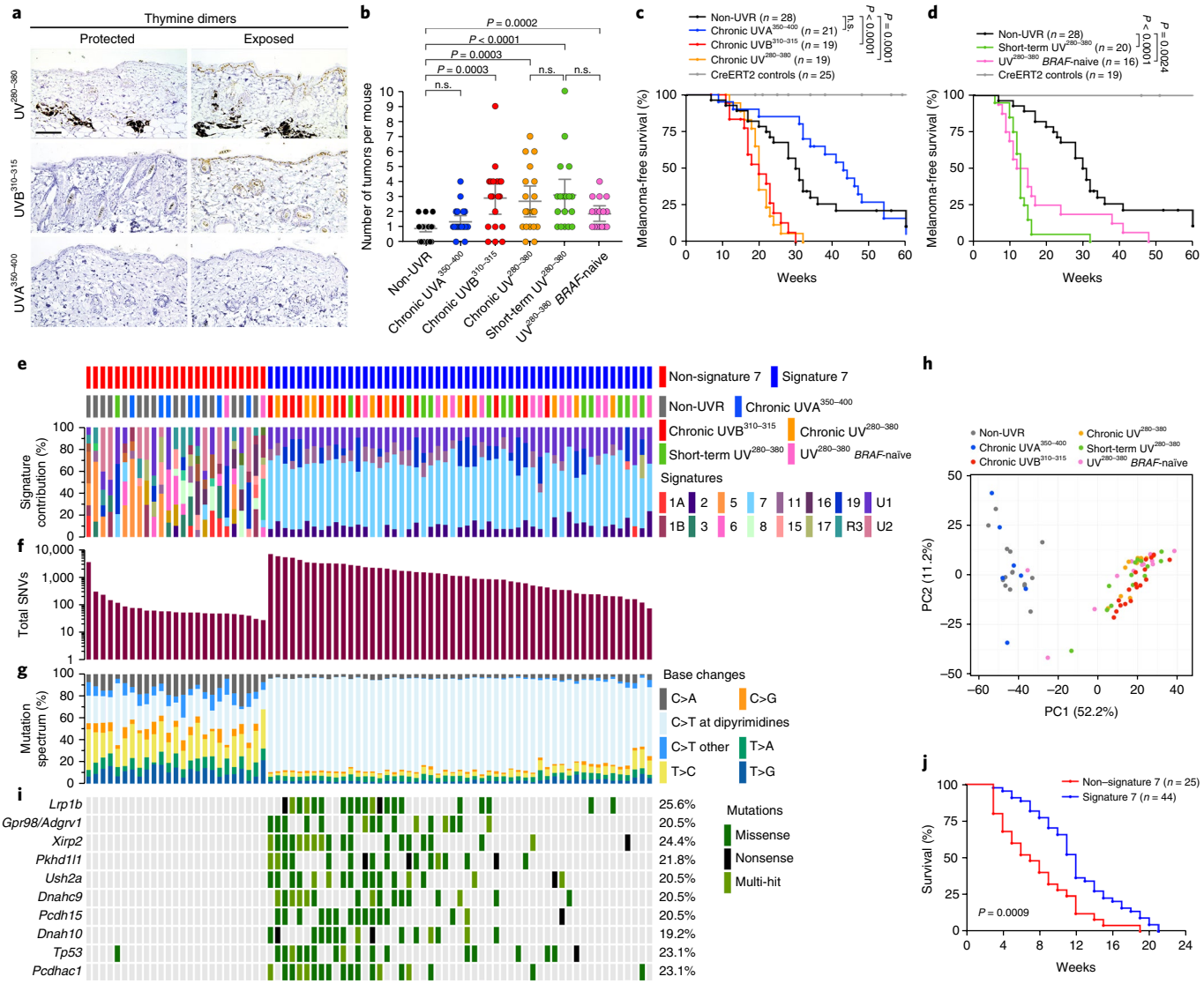

Fig. 2 | Signature 7 is imprinted by short-wavelength UVR and short-term UVR exposure. a, Photomicrographs of IHC for thymine dimers in protected and UVR-exposed sides of skin of *BRAF*^{V600E}-expressing mice 24 h after UV$^{280–380}$, UVB$^{310–315}$ or UVA$^{350–400}$ exposure. Scale bar, 50 µm. Representative of $n = 5$ animals per group. **b**, Mean tumor numbers in *BRAF*^{V600E} mice from the indicated treatment groups. The error bars show the mean ± 95% confidence interval; $n = 123$, two-tailed Mann–Whitney *U*-test. n.s., not significant. **c**,**d**, Melanoma-free survival of non-UVR and indicated UVR-exposed *BRAF*^{V600E} and CreERT2 mice (controls); two-tailed log-rank test. **e**–**g**, Classification of *BRAF*^{V600E}-driven mouse melanomas according to predominance of signature 7. The graphs represent the percentage of mutations attributed to each signature (**e**), total SNVs (**f**) and the spectrum of somatic base changes (**g**). **h**, PCA of mutational signature weights in mouse melanomas ($n = 78$). The values in parentheses denote the percentage of variance explained. **i**, Nonsynonymous mutations in mouse orthologs of the human genes presented in Fig. 1d. **j**, Survival of study mice from tumor appearance; two-tailed log-rank test.

UVR-exposed mice that did not express *BRAF*^{V600E} (controls) (Fig. 2c). Thus, UV$^{280–380}$ and UVB$^{310–315}$ accelerated melanomagenesis and increased tumor burden; most tumors (51 of 55) in these mice arose in the UVR-exposed areas. However, UVA$^{350–400}$ did not accelerate melanomagenesis, and tumors in these mice arose in the exposed (8 out of 28) and cloth-protected areas (Extended Data Fig. 4c).

Melanoma in early life is associated with childhood or adolescent sunburn[16], so to explore how limited UVR exposure affects melanomagenesis, mice expressing *BRAF*^{V600E} were exposed to UV$^{280–380}$ four times (short-term UV$^{280–380}$; Extended Data Fig. 4d). Surprisingly, these mice developed tumors with a median latency of 13 weeks, which is more rapid than in chronic UV$^{280–380}$-exposed mice ($P = 0.0001$; Fig. 2d and Supplementary Table 4), although without any difference in tumor burden ($P = 0.5040$; Fig. 2b). A high proportion of human naevi present *BRAF*^{V600E} mutations, suggesting that the *BRAF* mutation is an early event in melanomagenesis[17]. To explore the relationship between mutant *BRAF* and UVR, we treated mice with four UV$^{280–380}$ exposures before inducing *BRAF*^{V600E} (UV$^{280–380}$ *BRAF*-naive; Extended Data Fig. 4e). These mice developed more melanomas than non-UVR mice ($P = 0.0002$; Fig. 2b); intriguingly, the UV$^{280–380}$ *BRAF*-naive tumors arose with similar latency to short-term UV$^{280–380}$ tumors ($P = 0.2053$; Fig. 2d). Thus, UVR accelerated melanomagenesis even when administered before *BRAF*^{V600E} expression.

To define the mutational processes in our model, we performed whole-exome sequencing. Non-UVR-exposed and UVA$^{350–400}$ tumors did not present a particular mutational signature, whereas signature 7 predominated in all chronic UV$^{280–380}$ and UVB$^{310–315}$ tumors, and the majority of short-term UV$^{280–380}$ and UV$^{280–380}$ *BRAF*-naive tumors (Extended Data Fig. 5a), so we used our human

melanoma classification to segregate our mouse tumors. The non–signature 7 cohort included all non-UVR and $UVA^{350–400}$-exposed tumors, two $UV^{280–380}$ *BRAF*-naive tumors and one short-term $UV^{280–380}$ tumor (Fig. 2e). The signature 7 cohort included all chronic $UV^{280–380}$ and $UVB^{310–315}$ tumors, and the remaining 12 $UV^{280–380}$ *BRAF*-naive and 12 short-term $UV^{280–380}$ tumors (Fig. 2e). As in humans, the signature 7 mouse tumors presented more SNVs ($P<0.0001$) and a higher proportion of C-to-T transitions at dipyrimidines ($P<0.0001$; Fig. 2f,g and Extended Data Fig. 5b,c). PCA confirmed that this segregation was determined largely by signature 7 (Fig. 2h). Notably, mutations in the orthologous genes identified in human melanomas were also enriched in the mouse signature 7 melanomas, and these tumors also presented an increased abundance of predicted neoantigens (Fig. 2i and Extended Data Fig. 5d,e). Importantly, signature 7 tumor-–bearing mice presented a survival advantage from diagnosis over non–signature 7 tumor-bearing mice ($P=0.0009$; Fig. 2j).

Thus, we distinguish cutaneous melanomas by their underlying mutational processes, presumably representing distinct disease etiologies. Consistently, signature 7 is prognostic for outcome from diagnosis because patients with signature 7 tumors present better disease-free and overall survival than patients with non–signature 7 tumors. Signature 7 is associated with specific gene mutations that are also prognostic for survival. We validate our findings in a UVR-driven mouse melanoma model that recapitulates these cardinal features of human melanoma. Moreover, we reveal that signature 7 is associated with short wavelength UVR exposure and can be imprinted by only four UVR exposures. Finally, we uncover an intriguing plasticity whereby $BRAF^{V600E}$ and UVR cooperate to initiate melanoma irrespective of the order in which these events occur. Our studies emphasize the importance of prevention and education strategies to highlight the dangers of UVR and its carcinogenic role in melanoma.

Online content

Any methods, additional references, Nature Research reporting summaries, source data, statements of data availability and associated accession codes are available at https://doi.org/10.1038/s41591-018-0265-6.

Received: 11 December 2017; Accepted: 17 October 2018;
Published online: 3 December 2018

References

1. Whiteman, D. C. et al. *J. Natl. Cancer. Inst.* **95**, 806–812 (2003).
2. Day, C.-P., Marchalik, R., Merlino, G. & Michael, H. *Lab. Invest.* **97**, 698–705 (2017).
3. Akbani, R. et al. *Cell* **161**, 1681–1696 (2015).
4. Hayward, N. K. et al. *Nature* **545**, 175–180 (2017).
5. Krauthammer, M. et al. *Nat. Genet.* **44**, 1006–1014 (2012).
6. Brash, D. E. *Photochem. Photobiol.* **91**, 15–26 (2015).
7. Alexandrov, L. B. et al. *Nature* **500**, 415–421 (2013).
8. Rosenthal, R., McGranahan, N., Herrero, J., Taylor, B. S. & Swanton, C. *Genome Biol.* **17**, 31 (2016).
9. Hugo, W. et al. *Cell* **165**, 1–10 (2016).
10. Riaz, N. et al. *Cell* **171**, 1–16 (2017).
11. Rooney, M. S., Shukla, S. A., Wu, C. J., Getz, G. & Hacohen, N. *Cell* **160**, 48–61 (2015).
12. Gentles, A. J. et al. *Nat. Med.* **21**, 938–945 (2015).
13. El Ghissassi, F. et al. *Lancet Oncol.* **10**, 751–752 (2009).
14. Dhomen, N. et al. *Cancer Cell.* **15**, 294–303 (2009).
15. Viros, A. et al. *Nature* **511**, 478–482 (2014).
16. Whiteman, D. C., Whiteman, C. A. & Green, A. C. *Cancer Causes Control* **12**, 69–82 (2001).
17. Pollock, P. M. et al. *Nat. Genet.* **33**, 19–20 (2003).

Acknowledgements

This work was supported by CRUK-MI (A27412 and A22902) and the European Research Council (ERC Advanced Grant agreement No. 671262) to R.M. C.G-M. was supported by the French Society of Dermatology, UNICANCER and CEDEF. We acknowledge the contribution of the CRUK-MI core facilities and the contribution of the melanoma specimen donors.

Author contributions

L.D.T., P.A.M., P.G-M. and R.M. designed the study, analyzed the data and wrote the paper. K.H. designed and performed the experiments and analyzed the data. A.V. and N.D. contributed to study conception and design. A.K.M. and P.A.M. performed the bioinformatics analysis. D.A. provided technical assistance. N.M. and C.G-M. developed the clinical sample cohort. F.B., C.M. and B.S-L. performed the experiments. M.C. and A.V. performed the histological analysis.

Competing interests

R.M. is a consultant for Pfizer. All other authors declare no competing interests.

Additional information

Extended data is available for this paper at https://doi.org/10.1038/s41591-018-0265-6.

Supplementary information is available for this paper at https://doi.org/10.1038/s41591-018-0265-6.

Reprints and permissions information is available at www.nature.com/reprints.

Correspondence and requests for materials should be addressed to R.M.

Publisher's note: Springer Nature remains neutral with regard to jurisdictional claims in published maps and institutional affiliations.

Methods

Mutation signature analysis on human cutaneous melanomas. Mutation calls on the TCGA melanoma cohort ($n=467$) derived using the MuTect pipeline were downloaded from the Genomics Data Commons portal[18] (https://gdc-portal.nci.nih.gov). Clinical information on this cohort was downloaded from the cBioPortal for Cancer Genomics (http://www.cbioportal.org). Acral melanomas ($n=2$) and metastatic samples with unknown primary tumor origin ($n=35$) were filtered. We next performed a systematic review of the pathology reports and histological images of the remaining cases and removed an additional seven acral and four non-cutaneous melanomas that had been incorrectly annotated. The resultant cutaneous melanoma cohort ($n=419$) was analyzed with the deconstructSigs package[8] to determine the weights of mutation signatures. Predominance of signature 7 was defined in a given sample if signature 7 carried the maximum weight compared to each of the other individual signatures.

Data from two previously described cohorts of melanoma patients under immunotherapy[9,10] were downloaded from the National Center for Biotechnology Information (accession numbers: SRP067938/SRP090294 and SRP095809). For accession SRP067938/SRP090294 (37 samples, excluding cell lines), raw FASTQ files were processed through a standard pipeline consisting of low-quality read filtering through Trimmomatic (version 0.36), alignment to human genome GRCh37 using the Burrows–Wheeler Aligner (BWA, version 0.7.7) algorithm, marking PCR duplicates using picard (version 1.96) and the Genome Analysis Toolkit (GATK, version 3.6) corrections for realignments and mapping quality score recalibrations. For accession SRP095809 (44 cutaneous melanoma samples), somatic mutations were identified from BAM files with the MuTect algorithm (version 1.1.7). Mutational signatures were determined using the deconstructSigs package as described earlier.

Clinical samples and targeted sequencing. A prospective cohort study was performed through a collaboration between the Dermatology and Skin Cancer Department of La Timone Hospital (Marseille, France) and Cancer Research UK-Manchester Institute (CRUK-MI). Ethical approval was granted by the Assistance Publique des Hôpitaux de Marseille and Manchester Cancer Research Centre Biobank committees (reference number: 14-HTS12-02). Informed consent was obtained from all participants. We analyzed 126 primary cutaneous melanoma cases from patients diagnosed between January 2012 and September 2014. Tumor and germline DNA was extracted with GeneRead DNA FFPE kits (QIAGEN) from formalin-fixed, paraffin-embedded (FFPE) material after macrodissection of melanocytic neoplasm and adjoining healthy tissue, respectively. DNA integrity was assessed using the NGS FFPE QC Kit (Agilent Technologies) according to the manufacturer's instructions. Sequenced libraries were prepared from 10 to 200 ng of DNA from each sample using the SureSelect^{XT} Low Input Target Enrichment System (Agilent Technologies) designed to cover the coding exons of 17 genes of interest (*ADGRV1, BRAF, CDK4, CDKN2A, DNAH10, DNAH9, KIT, LRP1B, NF1, NRAS, PCDH15, PCDHAC1, PKHD1L1, POT1, TP53, USH2A* and *XIRP2*) following the manufacturer's protocol. Mutations in this gene set occur in 93% of TCGA melanoma samples. Libraries were equimolarly pooled and processed on a MiSeq System (Illumina), generating 150-bp paired-end reads with molecular barcodes. Raw FASTQ files were processed to remove low-quality reads and adapter contamination using SurecallTrimmer (version 4.0.1), available from Agilent Genomics Next Generation Toolkit. The resultant FASTQ files were aligned to the human reference genome (GRCh38) using the BWA aligner. Subsequently, the GATK was used for realignment around indels. PCR duplicates were removed using molecular barcode sequences with LocatIt (version 4.0.1) from Agilent Genomics Next Generation Tool kit. SAMtools (version 0.1.19) was used to convert the final BAM files (binary form of alignment output) to mpileup format. Variants were identified from mpileup files using VarScan (version 2.3.9) with *--min-coverage 50*, *--min-reads2 10* and *--min-var-freq 0.01*. Variants were subsequently processed using ProcessSomatic with *--max-normal-freq 0.005*. The final variants were annotated using Ensembl Variant Effect Predictor (VEP, version 85). Only samples with VEP annotations ($n=100$) were considered for the analysis.

Animal study. All procedures involving animals were performed in accordance with the ARRIVE (Animal Research: Reporting of In Vivo Experiments) guidelines and Home Office regulations under the Animals (Scientific Procedures) Act 1986 and under license PPL-70/7701. Procedures were approved by the Animal Welfare and Ethical Review Body of the CRUK-MI, and tumor volumes did not exceed the guidelines set by the Committee of the National Cancer Research Institute[19]. For genotyping, genomic DNA was prepared from ear biopsies, and PCR was performed using the primers previously described[14]. Tamoxifen (Sigma-Aldrich) was freshly prepared in 100% ethanol and applied to the shaven backs of 8- to 12-week-old mice to induce the expression of $BRAF^{V600E}$ in melanocytes of juvenile mice as previously described[14]. Four weeks later, back hair was shaved, and a UVR proof cloth was used to cover half of the back to provide an internal control. Mice were treated weekly with a single exposure of $UV^{280–380}$, $UVB^{310–315}$ or $UVA^{350–400}$ irradiation, for 4 weeks (short-term) or up to 6 months (chronic) depending on the setting, or until the animals developed melanoma. Mice were monitored for changes in skin appearance and the formation of tumors. For melanoma-free survival, time to first lesion was used. Animals were killed when their cumulative tumor burden reached a maximum of 1,500 mm^3 (determined by caliper measurements of tumor length (L), width (W) and depth (D), and calculated as volume $= L \times W \times D \times \pi / 6$), if they showed signs of ill health or distress or after a maximum of 24 months. Groups of >15 animals per cohort were selected to provide statistically significant survival rates in Kaplan–Meier analysis; randomization to groups was done by nonstatistical methods.

UVR treatment. Three Waldmann UV181 units (Athrodax Healthcare International Ltd) were fitted with UV6, TL-01 or UVA-1 lamps, emitting 280–380 nm, 310–315 nm and 350–400 nm wavelengths of UVR, respectively. A calibrated USB2000+ spectroradiometer (Ocean Optics) was used to measure the irradiance from the machines both before UV treatment and periodically as the treatments proceeded. A set of nine different positions within the field was measured to reliably determine the field-average irradiance, from which exposure times were calculated for the intended UVR doses. For the $UV^{280–380}$ and $UVB^{310–315}$ lamp, the doses where 1.6 kJ m^{-2} and 1.5 kJ m^{-2} erythema-weighted UVR, respectively, equivalent to 16 and 15 standard erythema doses, respectively. For the $UVA^{350–400}$ lamp, mice were exposed to 150 kJ m^{-2} unweighted UVR, the higher dose accounting for the lower energy.

Immunohistochemistry. Samples were fixed in 10% neutral buffered formalin for 24 h before processing. Organs were dehydrated through graded ethanol, cleared in xylene and embedded in paraffin wax; 4-µm sections were prepared, deparaffinized and stained with H&E. For IHC, sections were deparaffinized and rehydrated through graded alcohol. Heat-induced epitope retrieval was performed at 98 °C for 20 min, and slides were blocked with appropriate serum. Primary antibodies (mouse anti-p53 (1C12), Cell Signalling Technology; mouse anti-thymine dimer (clone KTM53), Kamiya Biomedical Company) were incubated at various concentrations for 30 min, followed by detection using a horseradish peroxidase polymer system with a 3,3′-diaminobenzine chromogen. Relevant antibody controls were used to assess positive and negative staining, and images were captured with a Leica DM4000 B LED microscope system.

Whole-exome sequencing. Snap-frozen tumor tissue was manually dissected by sectioning (25-µm thick) and DNA was extracted from sections with an estimated tumor cell percentage of at least 80% using the QIAGEN DNeasy kit according to the manufacturer's instructions. Germline DNA was isolated from the kidney. DNA quality was assessed using a Qubit 2.0 Fluorometer (Thermo Fisher Scientific). Exome capture was performed using the Agilent SureSelect Mouse All Exon V1 using 1 µg genomic DNA according to the manufacturer's instructions. Whole-exome sequencing was performed on the HiSeq 2500 system (Illumina) to produce 100-bp paired-end reads; the resultant D_FASTQ files were aligned to the mouse genome (GRCm38/mm10 release) using the BWA aligner. Duplicate reads were marked with picard, and the base quality score recalibration and local realignment around indels were performed using GATK. Somatic SNVs and indels were identified by comparing tumor–germline pairs using the VarScan software. Finally, the mutations were annotated for genetic context using Ensembl VEP (version 73), and variants present in the Single Nucleotide Polymorphism Database were excluded. A complete list of candidate nonsynonymous SNVs is provided (Supplementary Tables 5–11). The mutation signature analysis was performed using the deconstructSigs package[8]. PCAs were conducted using ClustVis[20].

Neoantigens prediction. For the subset of patients from the TCGA cutaneous melanoma cohort, tumor-specific neoantigen prediction data were available and obtained from Rooney et al.[11] For the murine melanomas, neoepitopes were predicted for each tumor by defining all possible 9-mer to 11-mer novel peptides resulting from missense mutations. The binding affinities of these mutant peptides and their corresponding wild-type peptide to the H2-Kb mouse alleles were predicted using the NetMHCpan server (version 4.0)[21]. Peptides with predicted binding strength <500 nM were considered as candidate neoantigens.

Statistics. For Kaplan–Meier survival analysis, a two-tailed log-rank test was used to determine the difference between groups. Nonparametric one- or two-tailed Mann–Whitney U-tests were performed using Prism version 7.00 (GraphPad). $P<0.05$ was considered significant.

Reporting Summary. Further information on research design is available in the Nature Research Reporting Summary linked to this article.

Data availability

All sequencing data generated that support the findings of this study have been deposited at the European Genome-phenome Archive (EGA) under accession number EGAS00001003243. All other relevant data are available from the corresponding author upon reasonable request.

References

18. Grossman, R. L. et al. *N. Engl. J. Med.* **375**, 1109–1112 (2016).
19. Workman, P. et al. *Br. J. Cancer* **102**, 1555–1577 (2010).
20. Metsalu, T. & Vilo, J. *Nucleic Acids Res.* **43**, W566–W570 (2015).
21. Jurtz, V. et al. *J. Immunol.* **199**, 3360–3368 (2017).
22. Charoentong, P. et al. *Cell Rep.* **18**, 248–262 (2017).
23. Newman, A. M. et al. *Nat. Methods* **12**, 453–457 (2015).

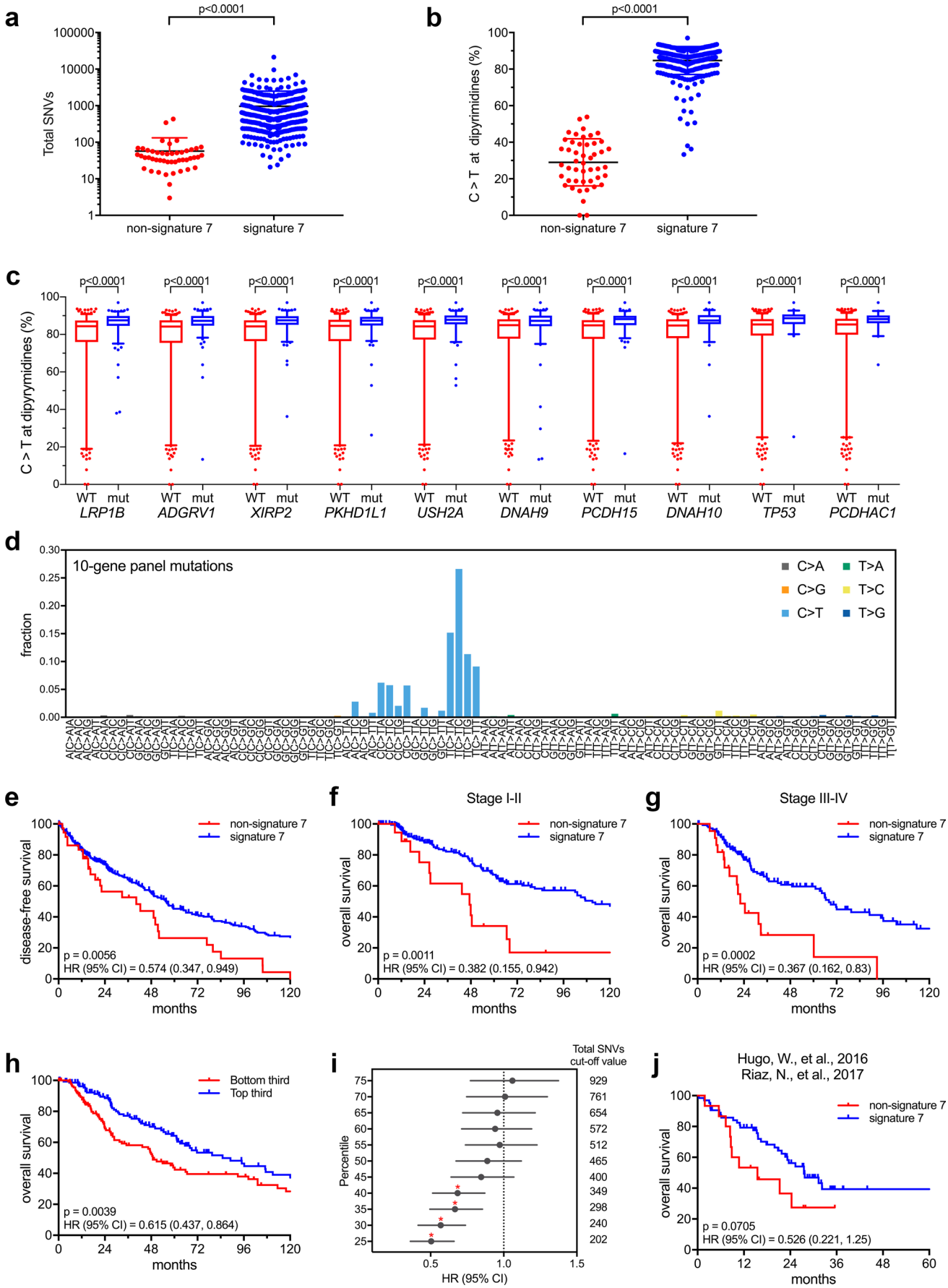

Extended Data Fig. 1 | See next page for caption.

Extended Data Fig. 1 | Signature 7 is associated with improved patient survival. a,**b**, Total number of SNVs (**a**) and proportion of C-to-T transitions at dipyrimidines (**b**) in non-signature 7 and signature 7 human melanomas from the TCGA dataset. Error bars show mean ± s.d.; $n = 419$, two-tailed Mann–Whitney test. **c**, Percentage of C-to-T nucleotide transitions in the TCGA human melanomas presenting wild-type (WT) or mutated (mut) alleles of the indicated genes. Boxes show median (25th–75th percentiles range), whiskers show 5th–95th percentiles range; $n = 419$, two-tailed Mann–Whitney test. **d**, Mutation signature for the 10-gene panel displayed as bar graphs showing the fraction of total mutations attributed to each of the 96-trinucleotide mutation types corresponding to a specific substitution and the sequence context adjacent to the mutated base. **e**, Disease-free survival comparing TCGA patients with non-signature 7 and signature 7 melanomas; $n = 365$, two-tailed log-rank test. **f**,**g**, Overall survival of TCGA patients with melanoma segregated according to signature 7 contribution and stratified by clinical stages I–II ($n = 212$) (**f**) and III–IV ($n = 165$) (**g**) based on the American Joint Committee on Cancer code (7th edition); two-tailed log-rank test. **h**, Overall survival of TCGA patients harboring melanomas with a high (top third) or low (bottom third) total number of mutations; $n = 273$, two-tailed log-rank test. **i**, Forest plot showing hazard ratio and 95% CI for overall survival for each cut-off value of total number of SNVs defined between the 25th and 75th percentiles; $n = 419$, $^*P < 0.05$, two-tailed log-rank test. **j**, Overall survival of cutaneous melanoma patients from combined Hugo, W. et al.[9] and Riaz, N. et al.[10] cohorts; $n = 80$, two-tailed log-rank test.

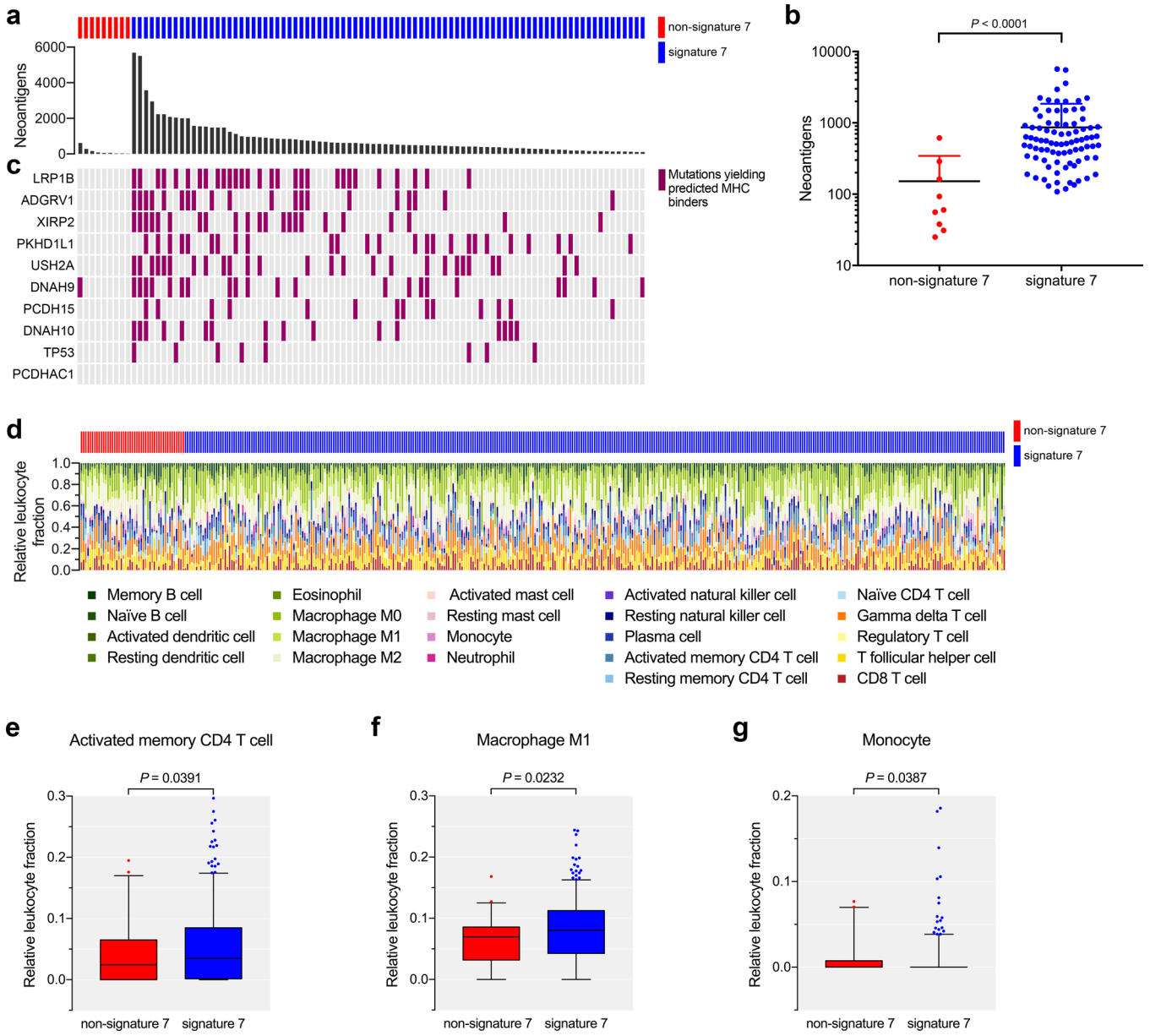

Extended Data Fig. 2 | Signature 7 correlates with more predicted neoantigens and a more favourable immune infiltrate composition. (**a**) Predicted neoantigen load of melanoma cases from TCGA (ref. 11) segregated into cohorts defined by the contribution of signature 7. (**b**) Number of predicted SNV-derived neoantigens in non-signature 7 vs. signature 7 human melanomas from TCGA; n = 419, two-tailed Mann-Whitney test. (**c**) Mutations in the 10-gene panel yielding high-binding affinity putative neoepitopes. (**d**) Relative leukocyte fractions of 22 immune cell subpopulations inferred from RNA-sequencing data[22] using the CIBERSORT deconvolution tool[23] in melanomas from TCGA. **e**,**f**,**g**, Distribution of estimated fractions of activated memory CD4 T cell (**e**), macrophage M1 (**f**) and monocyte (**g**) subsets in the non-signature 7 and signature 7 cohorts. Boxes show median (25th–75th percentiles range), whiskers show 5th–95th percentiles range; *n* = 418, one-tailed Mann-Whitney test.

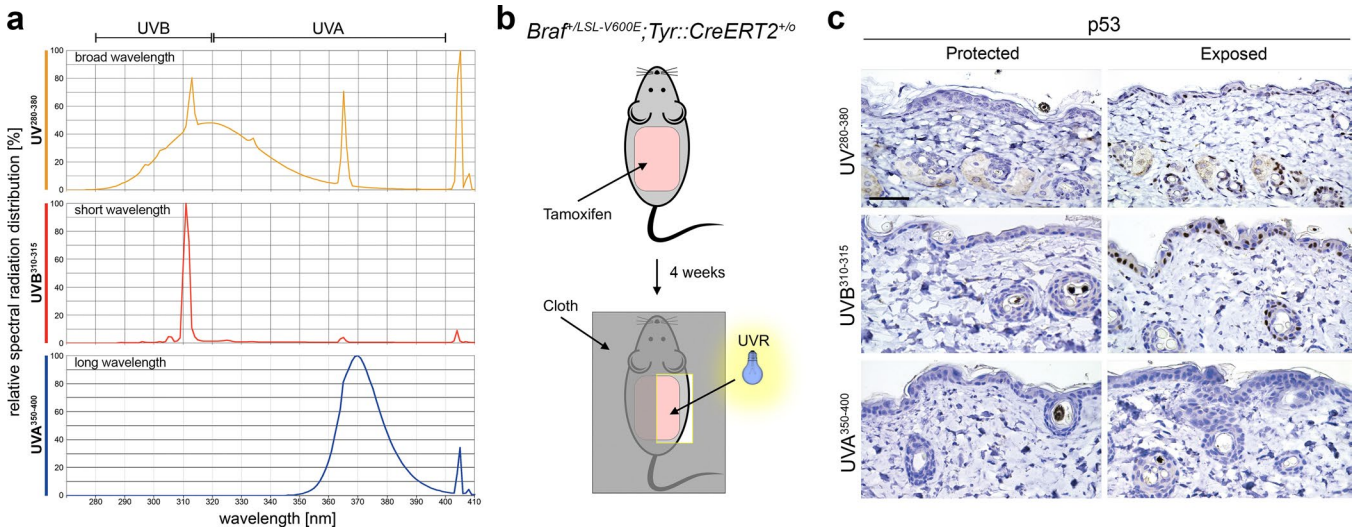

Extended Data Fig. 3 | p53 is induced by short wavelength UVR. a, Normalized spectral irradiance emitted from the $UV^{280-380}$, $UVB^{310-315}$ and $UVA^{350-400}$ lamps. **b**, Schematic representation of experimental design. **c**, Photomicrographs of IHC for p53 in the protected and contralateral $UV^{280-380}$, $UVB^{310-315}$ and $UVA^{350-400}$ exposed skins of $BRAF^{V600E}$-expressing mice 24 h after exposure. Scale bar, 30 μm. Representative of $n = 5$ animals per group.

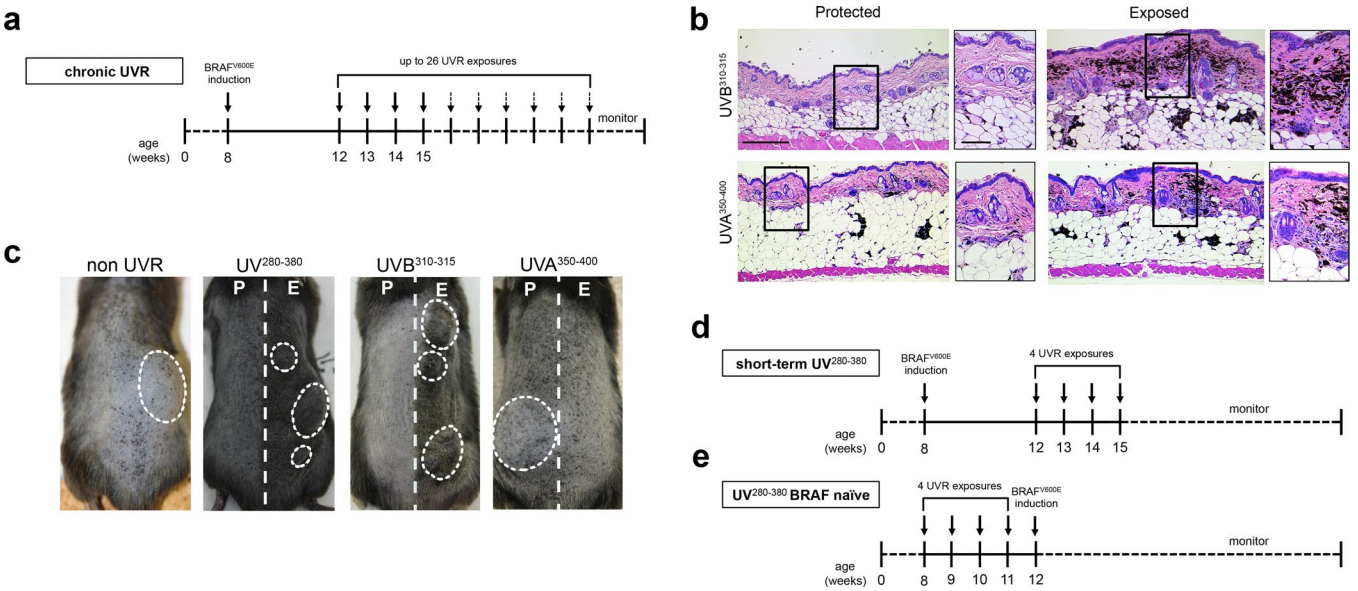

Extended Data Fig. 4 | Melanomagenesis is induced by short wavelength UVR. a, Schematic showing the experimental approach. In the chronic UVR cohorts, $BRAF^{V600E}$ was expressed in the melanocytes of 8-week-old mice using Cre-recombinase/*LoxP* technology. Four weeks later, mice were treated with UVR ($UV^{280-380}$, $UVB^{310-315}$ or $UVA^{350-400}$) weekly for up to 26 weeks (chronic exposure). **b**, Photomicrographs of H&E-stained skin sections from protected and UVR-exposed sides of the back of animals treated with $UVB^{310-315}$ or $UVA^{350-400}$. Scale bar, 300 μm. Right side panels are magnifications of boxed areas. Scale bar, 25 μm. Representative of all animals ($n = 40$) included in both cohorts. **c**, Photographs showing the macroscopic appearance of the skin of protected and UVR-exposed $BRAF^{V600E}$ mice when they reached tumour volume limits. Dashed lines divide the UVR protected (P) and exposed (E) areas. Individual tumors are highlighted by dotted lines. Representative of all animals ($n = 87$) included in each cohort. **d**,**e**, Schematics showing the experimental approach. For the short-term $UV^{280-380}$ cohort (**d**), $BRAF^{V600E}$ expression was induced at 8–12 weeks of age, and 4 weeks later mice were treated with UVR weekly for 4 weeks. For the $UV^{280-380}$ BRAF nave cohort (**e**), 8-week-old mice were exposed to UVR weekly for 4 weeks, followed by induction of $BRAF^{V600E}$ a week later.

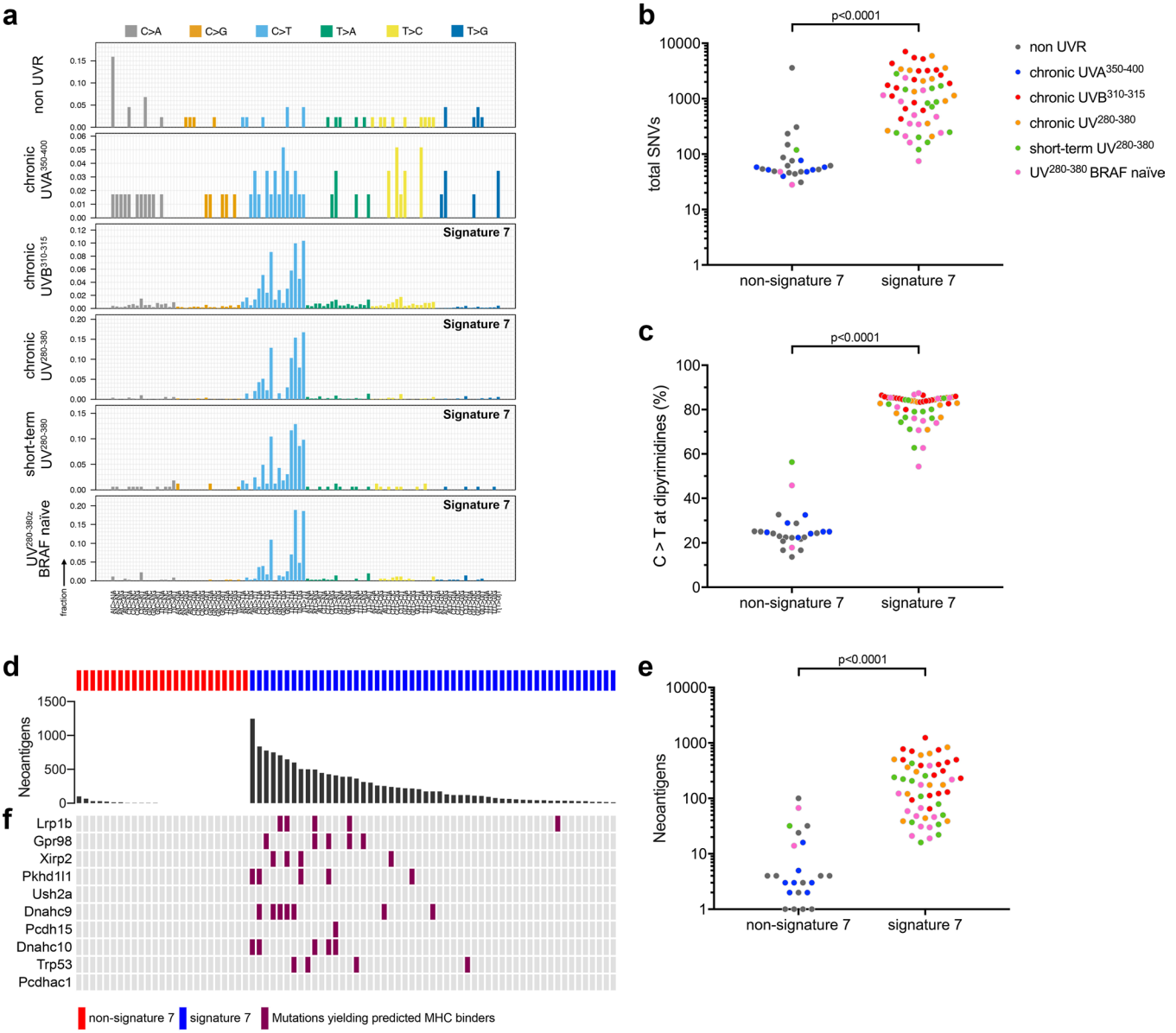

Extended Data Fig. 5 | Signature 7 is imprinted by short wavelength UVR. a, Examples of mutation signatures in mouse melanomas. Bar graphs show the fraction of total mutations attributed to each of the 96-trinucleotide mutation types corresponding to a specific substitution and the sequence context adjacent to the mutated base. Representative of all ($n=78$) sequenced tumours. **b**,**c**, Total number of SNVs (**b**) and proportion of C-to-T transitions at dipyrimidines (**c**) in non-signature 7 and signature 7 BRAF^{V600E} murine melanomas coloured by experimental cohort; $n=78$, two-tailed Mann–Whitney test. **d**, Predicted neoantigen load of mouse melanomas. **e**, Number of predicted SNV-derived neoantigens in non-signature 7 versus signature 7 mouse melanomas; $n=78$, two-tailed Mann–Whitney test. **f**, Mutations in the 10-gene panel yielding high-binding affinity putative neoepitopes.

nature research

Corresponding Author: Prof. Richard Marais

Date: Oct 4, 2018

Life Sciences Reporting Summary

Nature Research wishes to improve the reproducibility of the work we publish. This form is published with all life science papers and is intended to promote consistency and transparency in reporting. All life sciences submissions use this form; while some list items might not apply to an individual manuscript, all fields must be completed for clarity.

For further information on the points included in this form, see Reporting Life Sciences Research. For further information on Nature Research policies, including our data availability policy, see Authors & Referees and the Editorial Policy Checklist.

Experimental design

1. Sample size

Describe how sample size was determined.

We have used the TCGA melanoma cohort as a human cohort, hence no sample size calculation was performed.
Each mouse cohort included a minimum of 15 individuals, which were deemed to be sufficient to provide statistically significant survival rates comparisons based on our historical precedent (Viros et al., Nature, 2014).

2. Data exclusions

Describe any data exclusions.

Pre-established exclusion criteria was defined to only include cutaneous melanomas from the TCGA dataset in the analysis . Hence, samples that were reported as non-cutaneous melanomas, acral melanomas and metastatic melanomas of unknown primary tumour origin were excluded.
For the validation cohort, we analysed 126 primary cutaneous melanomas, and to account for high-confidence variant calling from sequencing reads, only samples with VEP annotations (n=100) were considered for the final analysis.
No experimental animals were excluded from the study.

3. Replication

Describe whether the experimental findings were reliably reproduced.

All UVR treatments followed standard operating protocols, and UVR machines were calibrated regularly to ensure the strength of UVR emission was consistent throughout experiments.
All histological assessments and immunostainings were perform in at least 5 mice per group and consistent results were obtained.

4. Randomization

Describe how samples/organisms/participants were allocated into experimental groups.

All mouse experiments were performed following standard operating protocols, and mice were allocated randomly to experimental groups on a rolling recruitment basis when they reached 8-12 weeks of age.

5. Blinding

Describe whether the investigators were blinded to group allocation during data collection and/or analysis.

The in vivo studies were not blinded, as there was limited technical capacity to perform the UVR experiments with blinding. Nonetheless, all experiments were performed on a rolling recruitment basis, thus the mice within each group had staggered start dates. Data regarding tumour free survival was collected weekly, but was only analysed in terms of survival on a monthly to bi-monthly basis. Due to staggered start dates and variable tumour free survival rates of each experimental group, survival was difficult to estimate until all the data had been collected.
Technicians were blinded during tumour size measurements in all experiments.
Investigators involved in the histopathological assessment were blinded during the analysis of the samples.

Note: all studies involving animals and/or human research participants must disclose whether blinding and randomization were used.

6. Statistical parameters

For all figures and tables that use statistical methods, confirm that the following items are present in relevant figure legends (or the Methods section if additional space is needed).

n/a	Confirmed	
☐	☒	The exact sample size (*n*) for each experimental group/condition, given as a discrete number and unit of measurement (animals, litters, cultures, etc.)
☐	☒	A description of how samples were collected, noting whether measurements were taken from distinct samples or whether the same sample was measured repeatedly.
☐	☒	A statement indicating how many times each experiment was replicated
☐	☒	The statistical test(s) used and whether they are one- or two-sided (note: only common tests should be described solely by name; more complex techniques should be described in the Methods section)
☐	☒	A description of any assumptions or corrections, such as an adjustment for multiple comparisons
☐	☒	The test results (e.g. *p* values) given as exact values whenever possible and with confidence intervals noted
☐	☒	A summary of the descriptive statistics, including central tendency (e.g. median, mean) and variation (e.g. standard deviation, interquartile range)
☐	☒	Clearly defined error bars

See the web collection on statistics for biologists for further resources and guidance.

Software

Policy information about availability of computer code

7. Software

Describe the software used to analyze the data in this study.

We have used BWA aligner (v 0.7.7), Picard (v 1.107 and 1.96), GATK (v 3.1 and 3.6), SureCallTrimmer (v. 4.0.1), LocatIT (v. 4.0.1), Samtools (v. 0.1.19) VarScan (v 2.3.6 and 2.3.9), Variant Effect Predictor (Ensembl version 73 and 85) and MuTect (v. 1.1.7) in the analysis of WES and targeted sequencing data. All the mutation signatures were calculated using deconstructSigs package in R. Principal component analyses were conducted using ClustVis (https://biit.cs.ut.ee/clustvis/). Statistical tests were performed using GraphPad Prism version 7.00

For all studies, we encourage code deposition in a community repository (e.g. GitHub). Authors must make computer code available to editors and reviewers upon request. The *Nature Methods* guidance for providing algorithms and software for publication may be useful for any submission.

Materials and reagents

Policy information about availability of materials

8. Materials availability

Indicate whether there are restrictions on availability of unique materials or if these materials are only available for distribution by a for-profit company.

The genetically engineered BRAF(V600E) mouse model is available from the corresponding author upon reasonable request.

9. Antibodies

Describe the antibodies used and how they were validated for use in the system under study (i.e. assay and species).

Primary antibodies [Mouse anti-p53 (clone 1c12), Cell signalling (cat. #2524), dilution 1:500; Mouse anti-thymine dimer (clone KTM53), Kamiya Biomedical Company (cat. #MC-062), dilution 1:200] were used as recommended by the manufacturers, respectively (see https://media.cellsignal.com/pdf/2524.pdf and http://www.hoelzel-biotech.com/media/import/pdf_manual/Kamiya//MC-062__Manual.pdf). The antibodies were previously validated by the producers. Relevant isotype controls were included in each run to confirm positive and negative staining.

10. Eukaryotic cell lines

a. State the source of each eukaryotic cell line used.

no eukaryotic cell lines were used

b. Describe the method of cell line authentication used.

no eukaryotic cell lines were used

c. Report whether the cell lines were tested for mycoplasma contamination.

no eukaryotic cell lines were used

d. If any of the cell lines used in the paper are listed in the database of commonly misidentified cell lines maintained by ICLAC, provide a scientific rationale for their use.

no eukaryotic cell lines were used

Animals and human research participants

Policy information about studies involving animals; when reporting animal research, follow the ARRIVE guidelines

11. Description of research animals

Provide details on animals and/or animal-derived materials used in the study.

Braf(+/LSL-V600E);Tyr::CreERT2(+/o) line was back-crossed over ten generations to C57BL/6J. Mice were recruited onto experiments at 6-8 weeks of age. For experiments <5 weeks long (schematics in Ext. Data Fig. 3b), both male and female mice were used. For experiments >5 weeks long (schematics in Ext. Data Fig. 4), female mice were used.

Policy information about studies involving human research participants

12. Description of human research participants

Describe the covariate-relevant population characteristics of the human research participants.

For the validation study we analyzed primary tumours from patients diagnosed with cutaneous melanoma between January 2012 and September 2014. The median age of diagnosis of the patients was 62 years (range: 19-87 years), with a distribution of 45% females and 55% men. Sixty cases where diagnosed with superficial spreading melanoma, 38 were nodular melanomas and 2 cases were non assessable. Thirty seven patients presented with disease stage I, 37 with stage II, 25 with stage III and one patient presented with stage IV.